This is the accepted manuscript made available via CHORUS. The article has been published as:

Inversion of Qubit Energy Levels in Qubit-Oscillator Circuits in the Deep-Strong-Coupling Regime

F. Yoshihara, T. Fuse, Z. Ao, S. Ashhab, K. Kakuyanagi, S. Saito, T. Aoki, K. Koshino, and K. Semba

Phys. Rev. Lett. **120**, 183601 — Published 3 May 2018
DOI: 10.1103/PhysRevLett.120.183601

Inversion of qubit energy levels in qubit-oscillator circuits in the deep-strong-coupling regime

F. Yoshihara,[1,*] T. Fuse,[1] Z. Ao,[2] S. Ashhab,[3] K. Kakuyanagi,[4] S. Saito,[4] T. Aoki,[2] K. Koshino,[5] and K. Semba[1,†]

[1]*Advanced ICT Institute, National Institute of Information and Communications Technology, 4-2-1, Nukuikitamachi, Koganei, Tokyo 184-8795, Japan*

[2]*Department of Applied Physics, Waseda University, 3-4-1, Ookubo, Shinjuku-ku, Tokyo, Japan*

[3]*Qatar Environment and Energy Research Institute, Hamad Bin Khalifa University, Qatar Foundation, Doha, Qatar*

[4]*NTT Basic Research Laboratories, NTT Corporation, 3-1 Morinosato-Wakamiya, Atsugi, Kanagawa 243-0198, Japan*

[5]*College of Liberal Arts and Sciences, Tokyo Medical and Dental University, 2-8-30, Kounodai, Ichikawa, Chiba 272-0827, Japan.*

(Dated: March 27, 2018)

We report on experimentally measured light shifts of superconducting flux qubits deep-strongly coupled to LC oscillators, where the coupling constants are comparable to the qubit and oscillator resonance frequencies. By using two-tone spectroscopy, the energies of the six lowest levels of each circuit are determined. We find huge Lamb shifts that exceed 90% of the bare qubit frequencies and inversions of the qubits' ground and excited states when there are a finite number of photons in the oscillator. Our experimental results agree with theoretical predictions based on the quantum Rabi model.

According to quantum theory, the vacuum electromagnetic field has "half photon" fluctuations, which cause several physical phenomena such as the Lamb shift [1]. A cavity can enhance the interaction between the atom and the electromagnetic field inside the cavity, and enables more precise measurements on the influence of the vacuum. Cavity/circuit-quantum electrodynamics (QED) systems are well described by the Jaynes-Cummings Hamiltonian [2, 3]. In the strong coupling regime, when the cavity's resonance frequency ω is on resonance with the atom's transition frequency Δ, the vacuum Rabi splitting [4–6] and oscillation [7, 8] have been observed. In the off-resonance case, the Lamb shift [9–11] caused by the vacuum fluctuations, and the ac-Stark shift proportional to the photon number in the cavity, were observed [10–13]. In the so-called ultrastrong coupling regime [14, 15], where the coupling constant g becomes around 10% of Δ and ω, and the deep-strong-coupling regime [16, 17], where g is comparable to or larger than Δ and ω, the rotating-wave approximation used in the Jaynes-Cummings Hamiltonian breaks down and the system should be described by the quantum Rabi Hamiltonian [18–20]. In these regimes, the light shifts of an atom could non-monotonously change as g increases, and the amount of the shift is not proportional to the photon number in the cavity [21, 22].

In this work, to study the light shift in the case of $g \sim \omega$, we investigated qubit-oscillator circuits that each comprises a superconducting flux qubit [23] and an LC oscillator inductively coupled to each other by sharing a loop of Josephson junctions that serves as a coupler [Figs. 1(a) and (c)]. By using two-tone spectroscopy [24, 25], energies of the six lowest energy eigenstates were measured, and the photon-number-dependent qubit frequencies were evaluated. We find Lamb shifts over 90% of the bare qubit frequency and inversions of the qubit's ground and the excited states when there are a finite number of photons in the oscillator.

The qubit-oscillator circuit is described by the Hamiltonian

$$\hat{H} = -\frac{\hbar}{2}(\Delta\hat{\sigma}_x + \varepsilon\hat{\sigma}_z) + \hbar\omega\hat{a}^\dagger\hat{a} + \hbar g\hat{\sigma}_z\left(\hat{a} + \hat{a}^\dagger\right). \quad (1)$$

The first two terms represent the energy of the flux qubit written in the basis of two states with persistent currents flowing in opposite directions around the qubit loop, $|\circlearrowleft\rangle_\mathrm{q}$ and $|\circlearrowright\rangle_\mathrm{q}$. The operators $\hat{\sigma}_{x,z}$ are the standard Pauli operators. The parameters $\hbar\Delta$ and $\hbar\varepsilon$ are the tunnel splitting and the energy bias between $|\circlearrowleft\rangle_\mathrm{q}$ and $|\circlearrowright\rangle_\mathrm{q}$, where $\hbar\varepsilon$ can be controlled by the flux bias through the qubit loop Φ_q. The third term represents the energy of the LC oscillator, where $\omega = 1/\sqrt{(L_0 + L_\mathrm{c})C}$ [see Fig. 1(a)] is the resonance frequency, and $\hat{a}^\dagger$ and $\hat{a}$ are the creation and annihilation operators, respectively. The fourth term represents the coupling energy.

At $\varepsilon = 0$, the Hamiltonian in Eq. (1) is equivalent to that of the quantum Rabi model $\hat{H}_\mathrm{Rabi}$. In the limit $\Delta \ll \omega$, the energy eigenstates are well described by Schrödinger-cat-like entangled states between persistent-current states of the qubit and displaced Fock states of the oscillator $\hat{D}(\pm\alpha)|n\rangle_\mathrm{o}$ [21, 22]:

$$|\mathrm{g}n\rangle \simeq \frac{|\circlearrowleft\rangle_\mathrm{q} \otimes \hat{D}(-\frac{g}{\omega})|n\rangle_\mathrm{o} + |\circlearrowright\rangle_\mathrm{q} \otimes \hat{D}(\frac{g}{\omega})|n\rangle_\mathrm{o}}{\sqrt{2}},$$

$$|\mathrm{e}n\rangle \simeq \frac{|\circlearrowleft\rangle_\mathrm{q} \otimes \hat{D}(-\frac{g}{\omega})|n\rangle_\mathrm{o} - |\circlearrowright\rangle_\mathrm{q} \otimes \hat{D}(\frac{g}{\omega})|n\rangle_\mathrm{o}}{\sqrt{2}}. \quad (2)$$

Here, $\hat{D}(\alpha) = \exp(\alpha\hat{a}^\dagger - \alpha^*\hat{a})$ is the displacement operator, and α is the amount of the displacement. The

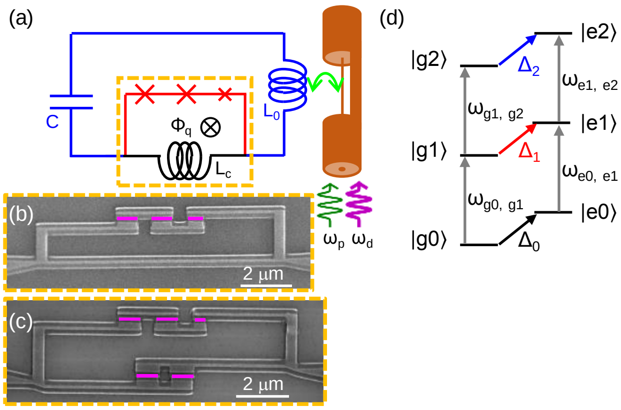

FIG. 1. (a) Circuit diagram. A superconducting flux qubit (red and black) and a superconducting LC oscillator (blue and black) are inductively coupled to each other by sharing an inductance (black). (b), (c) Scanning microscope images of the qubit and the shared inductance located at the orange rectangle in diagram (a). Josephson junctions are represented by magenta rectangles. The shared inductance is a superconducting lead (b) or a loop of Josephson junctions (c). (d) The diagram of the six lowest energy-levels of a qubit-oscillator circuit. The energy eigenstates are expressed as $|in\rangle$ ($i =$ g, e and $n = 0, 1, 2, \cdots$), which indicates that the qubit is in "g" the ground or "e" the excited state and the number of real photons in the oscillator is n. The arrows indicate transition frequencies between energy eigenstates and also mean that the transitions are allowed. Here, Δ_n ($n = 0, 1, 2$) is the photon-number-dependent qubit frequency.

energy eigenstates on the left-hand side are expressed as $|in\rangle$ ($i =$ g, e), where "g" and "e" denote, respectively, the ground and excited states of the qubit and n the number of real photons in the oscillator. On the right-hand side, $|n\rangle_{\rm o}$ denotes the oscillator's n-photon Fock state. Note that the displaced vacuum state $\hat{D}(\alpha)|0\rangle_{\rm o}$ is the coherent state $|\alpha\rangle_{\rm o} = \exp(-|\alpha|^2/2)\sum_{n=0}^{\infty}\alpha^n|n\rangle_{\rm o}/\sqrt{n}$.

The photon-number-dependent qubit frequency $\Delta_n(g/\omega) \equiv \omega_{{\rm e}n} - \omega_{{\rm g}n}$ is defined as the energy difference between the energy eigenstates $|{\rm g}n\rangle$ and $|{\rm e}n\rangle$, and it can be expressed as [see the solid lines in Fig. 4]:

$$\begin{aligned}\Delta_n(g/\omega) &= \langle {\rm e}n|\hat{H}_{\rm Rabi}|{\rm e}n\rangle - \langle {\rm g}n|\hat{H}_{\rm Rabi}|{\rm g}n\rangle \\ &\simeq \Delta[{}_{\rm o}\langle n|\hat{D}^{\dagger}(-g/\omega)\hat{D}(g/\omega)|n\rangle_{\rm o}] \\ &= \Delta\exp(-2g^2/\omega^2)L_n(4g^2/\omega^2). \qquad (3)\end{aligned}$$

Here, L_n is a Laguerre polynomial; $L_0(x) = 1$, $L_1(x) = 1 - x$, $L_2(x) = (x^2 - 4x + 2)/2$, and so on. The difference between Δ_n and the bare qubit frequency Δ can be considered as the n-photon ac-Stark shifts $|\Delta_n - \Delta|$. In particular, $|\Delta_0 - \Delta|$ is referred to as the Lamb shift. Note that the Bloch-Siegert shift [26, 27], the contribution from the counter-rotating terms, is included in the n-photon ac-Stark shifts. Since $L_0 = 1$, a considerable Lamb shift is expected when g becomes comparable to ω. A similar suppression of transition frequencies because of coupling to other degrees of freedom is well known in polaron physics and other fields. For example such an effect was recently discussed for an Andreev-level qubit [28]. Considering that L_n has n zeros, i.e. points where $L_n(x)$ is equal to zero, $\Delta_n(x)$ also has n zeros, and hence, in general alternates between positive and negative values. In other words, the qubit's ground and excited states exchange their roles everytime when $\Delta_n = 0$. The bare qubit frequency Δ is the tunnel energy between the states $|\circlearrowleft\rangle_{\rm q}$ and $|\circlearrowright\rangle_{\rm q}$. Taking either one of these two states and a finite value of g, the oscillator is populated by virtual photons even in the ground state, and the virtual photon states for the qubit states $|\circlearrowleft\rangle_{\rm q}$ and $|\circlearrowright\rangle_{\rm q}$ are different from each other. As a result, the qubit has to "drag" the oscillator every time it flips its state, which can be seen as an effective reduction of Δ by a factor that is determined by the overlap integral between the interaction-caused displaced n-photon Fock states of the oscillator [29] as described by the second line of Eq. (3). One way to understand negative values of Δ_n is to think of them as describing a situation where the anti-bonding state of $|\circlearrowleft\rangle_{\rm q}$ and $|\circlearrowright\rangle_{\rm q}$ is more stable than the bonding state. Note that here the displaced states $\hat{D}(\pm g/\omega)|0\rangle_{\rm o}$ contain only virtual photons while the states $\hat{D}(\pm g/\omega)|n\rangle_{\rm o}$ for $n \geq 1$ contain a mixture of real and virtual photons.

Although Eqs. (2) and (3) are not exact for general values of the circuit parameters, they remain reasonably good approximations as long as $\Delta < \omega$. Furthermore, the symmetry of $\hat{H}_{\rm Rabi}$ is independent of the circuit parameters, which means that certain transitions will remain forbidden even if the corresponding states do not have simple forms. These two considerations allow us to easily identify the energies of the different eigenstates from the experimental spectra [29].

To determine the parameters of the qubit-oscillator circuits (Δ, ω, and g), spectroscopy was performed by measuring the transmission spectrum through the transmission line that is inductively coupled to the LC oscillator [Fig. 1(a)]. In total, nine sets of parameters (A–I in Table I) in five circuits were evaluated. The shared inductance of the circuit for set A is a superconducting lead [Fig. 1(b)], while that of the circuits for sets B–I is a loop of Josephson junctions [Fig. 1(c)], where eight flux bias points in four circuits were used [29]. Therefore, much larger g is expected for sets B–I. When the frequency of the probe signal $\omega_{\rm p}$ matches the frequency ω_{kl} of a transition $|k\rangle \to |l\rangle$, where $|0\rangle$ stands for the ground state and $|k\rangle$ with $k \geq 1$ stands for the kth excited state of the coupled circuit, the transmission amplitude decreases, provided that the transition matrix element $\langle k|(\hat{a} + \hat{a}^{\dagger})|l\rangle$ is not 0. Note that for nonzero values of ε, we have labeled the energy eigenstates using a single integer k instead of the label $|in\rangle$ used above. Figure 2 shows the amplitudes of the transmission spectra $|S_{21}^{\rm meas}(\varepsilon, \omega_{\rm p})/S_{21}^{\rm bg}(\omega_{\rm p})|$ for sets A and H. Here, $\omega_{\rm p}$ is the probe frequency, and $S_{21}^{\rm meas}(\varepsilon, \omega_{\rm p})$ and $S_{21}^{\rm bg}(\omega_{\rm p})$ are respectively measured and

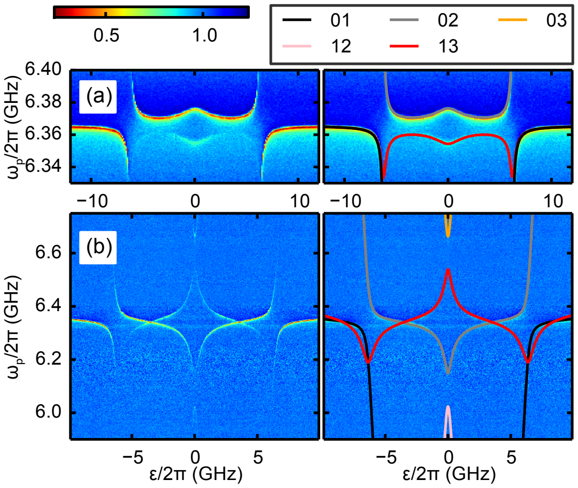

FIG. 2. Measured transmission spectra for two qubit-oscillator circuits as functions of the qubit's energy bias ε and probe frequency ω_{p}. The color scheme is chosen such that the lowest point in each spectrum is red and the highest point is blue. The right panels show the transition frequencies calculated from the Hamiltonian to fit experimental data. The black, gray, orange, pink, and red lines correspond to the transitions $|0\rangle \to |1\rangle$, $|0\rangle \to |2\rangle$, $|0\rangle \to |3\rangle$, $|1\rangle \to |2\rangle$, and $|1\rangle \to |3\rangle$, respectively. The parameters are obtained as (a) $\Delta/2\pi = 1.246$ GHz, $\omega/2\pi = 6.365$ GHz, and $g/2\pi = 0.42$ GHz corresponding to set A; (b) $\Delta/2\pi = 1.68$ GHz, $\omega/2\pi = 6.345$ GHz, and $g/2\pi = 7.27$ GHz corresponding to set H.

	$\frac{\Delta}{2\pi}$	$\frac{\omega}{2\pi}$	$\frac{g}{2\pi}$	$\frac{\Delta_0}{2\pi}$	$\frac{\Delta_1}{2\pi}$	$\frac{\Delta_2}{2\pi}$
A	1.246	6.365	0.42	1.236	1.215	
				(1.235)	(1.213)	
B	1.01	6.296	5.41	0.233	−0.452	−0.13
				(0.229)	(−0.448)	(−0.123)
C	0.92	6.288	5.59	0.193	−0.412	−0.062
				(0.189)	(−0.410)	(−0.059)
D	3.93	5.282	5.28	0.54	−1.512	0.56
				(0.539)	(−1.503)	(0.624)
E	4.88	5.230	5.37	0.607	−1.746	0.906
				(0.607)	(−1.741)	(1.018)
F	4.71	5.220	5.46	0.538	−1.642	1.005
				(0.542)	(−1.641)	(1.087)
G	3.53	5.263	5.58	0.375	−1.255	0.8
				(0.379)	(−1.244)	(0.834)
H	1.68	6.345	7.27	0.127	−0.518	0.5
				(0.122)	(−0.514)	(0.523)
I	1.61	6.335	7.48	0.099	−0.458	0.493
				(0.099)	(−0.451)	(0.532)

TABLE I. Parameters of qubit-oscillator circuits in GHz. Δ, ω, and g are obtained from the (single-tone) transmission spectra. The numbers for Δ_n (n = 0, 1, 2) in the upper line for each data set are obtained from two-tone transmission spectra, while those in the lower line (i.e. those between parentheses) are numerically calculated values using $\hat{H}_{\mathrm{Rabi}}$ and the parameters Δ, ω, and g.

background transmission coefficients [29].

The parameters are obtained from fitting the experimentally measured resonance frequencies to those numerically calculated by diagonalizing $\hat{H}$ with Δ, ω and g treated as fitting parameters. In Fig. 2, the right panels show the calculated transition frequencies superimposed on the measured spectra. In Fig. 2(a), one can see the splitting of $|0\rangle \to |2\rangle$ and $|1\rangle \to |3\rangle$ transition frequencies around $\varepsilon = 0$, known as the qubit-state-dependent frequency shifts of the oscillator. From the fitting, the parameters are obtained as $\Delta/2\pi = 1.246$ GHz, $\omega/2\pi = 6.365$ GHz, and $g/2\pi = 0.42$ GHz. The spectrum shown in Fig. 2(b) looks qualitatively different from that in (a) as discussed in Ref. [17]. The parameters are obtained as $\Delta/2\pi = 1.68$ GHz, $\omega/2\pi = 6.345$ GHz, and $g/2\pi = 7.27$ GHz. Here, g is larger than both Δ and ω, indicating that the circuit is in the deep-strong-coupling regime [$g \gtrsim \max(\omega, \sqrt{\Delta\omega}/2)$] [21, 30, 31]. The parameters from all the sets are summarized in Table I.

To obtain the photon-number-dependent qubit frequency Δ_n (n = 0, 1, 2), at least five transition frequencies out of seven allowed transitions [Fig. 1(d)] are necessary. However, in each spectrum at $\varepsilon = 0$, we see only two signals at frequencies $\omega_{\mathrm{g0,g1}}$ and $\omega_{\mathrm{e0,e1}}$ respectively corresponding to the transitions $|\mathrm{g0}\rangle \to |\mathrm{g1}\rangle$ and $|\mathrm{e0}\rangle \to |\mathrm{e1}\rangle$, which were also observed in our previous experiments [16, 17]. There are two main reasons behind this limitation on single-tone spectroscopy, where only a single-frequency weak probe signal is applied to the circuit. First, only transition frequencies in the range of the measurement setup (in our case 4 to 8 GHz) can be measured. Second, the signal from transitions that do not start from the lowest two energy levels will be weak because of the small thermal population of higher energy levels (in our case the thermal population decreases by two orders of magnitude for each step up in the value of n).

To access transitions other than $|\mathrm{g0}\rangle \to |\mathrm{g1}\rangle$ and $|\mathrm{e0}\rangle \to |\mathrm{e1}\rangle$, two-tone spectroscopy was used, where a drive signal with frequency ω_{d} is applied while the transmission of a probe signal with frequency ω_{p} around the frequency $\omega_{\mathrm{g0,g1}}$ or $\omega_{\mathrm{e0,e1}}$ is measured. When ω_{d} is equal to the frequency of an allowed transition involving at least one of the states $|\mathrm{g0}\rangle$, $|\mathrm{g1}\rangle$, $|\mathrm{e0}\rangle$, and $|\mathrm{e1}\rangle$, an Autler-Townes splitting [32] takes place and is observed in the probe transmission signal. Figure 3 shows the measured two-tone transmission spectra from set H. An avoided crossing between a horizontal line and a diagonal line [29] is observed in each panel. Interestingly, the slope of the diagonal line is $\partial\omega_{\mathrm{p}}/\partial\omega_{\mathrm{d}} = -1$ for panels (a) and (b), and $+1$ for panel (c), which indicates that the absorption of

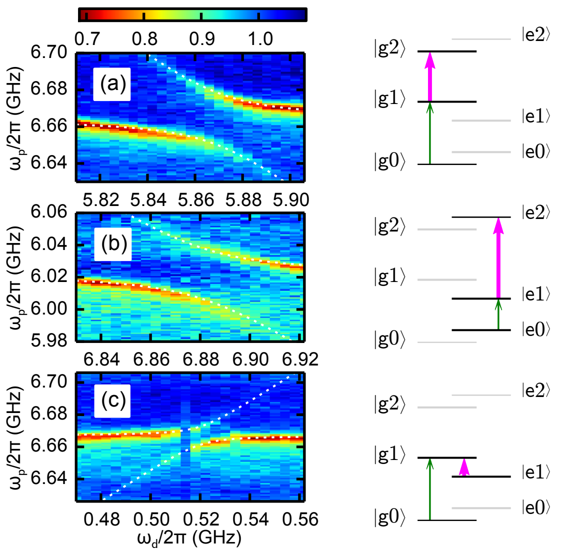

FIG. 3. (left) Measured two-tone transmission spectra as functions of drive frequency $\omega_{\rm d}$ and probe frequency $\omega_{\rm p}$. The color scheme is chosen such that the lowest point in each spectrum is red and the highest point is blue. The white dotted lines are calculated transition frequencies considering dressed states due to the drive signals. The right panels show the energy-level diagrams. The thin green arrows indicate transitions scanned by the probe signal, while thick magenta arrows indicate transitions scanned by drive signals.

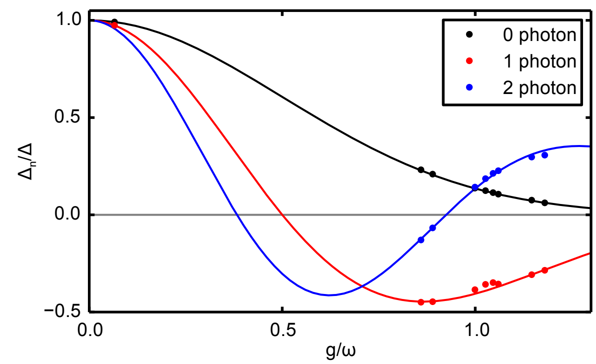

FIG. 4. Photon-number-dependent normalized qubit frequencies Δ_n/Δ as functions of g/ω. The parameters Δ, ω, and g are obtained from the (single-tone) transmission spectra. The black, red, and blue solid circles are respectively the qubit frequencies Δ_0, Δ_1, and Δ_2 obtained from the two-tone transmission spectra. The solid lines are Δ_n obtained from Eq. (3).

one probe photon is accompanied by the absorption of one photon from the drive field in panels (a) and (b) and the emission of one photon to the drive field in panel (c). Together with the frequencies numerically calculated from $\hat{H}_{\rm Rabi}$, the corresponding transitions are identified as shown in the right-hand side of each spectrum. The spectrum in panel (c) demonstrates that the energy of $|{\rm g1}\rangle$ is higher than that of $|{\rm e1}\rangle$ and hence Δ_1 is negative. In other words, the qubit's energy levels are inverted.

Moreover, from these three two-tone transmission spectra, five transition frequencies, $\omega_{\rm g0,g1}$, $\omega_{\rm g0,g2}$, $\omega_{\rm e0,e1}$, $\omega_{\rm e0,e2}$, and $\omega_{\rm g0,e1}$, can be evaluated; In panel (a), the horizontal line corresponds to a one-photon resonance, $\omega_{\rm p} = \omega_{\rm g0,g1}$, whereas the diagonal line corresponds to a two-photon resonance, $\omega_{\rm p} = \omega_{\rm g0,g2} - \omega_{\rm d}$. For panel (b), similarly, the horizontal line is at $\omega_{\rm p} = \omega_{\rm e0,e1}$ and the diagonal line is at $\omega_{\rm p} = \omega_{\rm e0,e2} - \omega_{\rm d}$. For panel (c), the horizontal line is at $\omega_{\rm p} = \omega_{\rm g0,g1}$ and the diagonal line is at $\omega_{\rm p} = \omega_{\rm g0,e1} + \omega_{\rm d}$. From these five transition frequencies, all the eigenenergies up to the fifth-excited state can be determined, up to an overall energy shift. One thing is worth emphasizing here. In the two-tone spectroscopy of a deep-strongly-coupled qubit-oscillator circuit, the states of the qubit are doubly dressed: one is the conventional dressing by the classical drive field while the other is in the quantum regime due to deep-strong coupling to the oscillator, where the oscillator's states are displaced. The experimental results demonstrate that the two kinds of dressed states coexist.

From Eq. (3), the normalized photon-number-dependent qubit frequencies Δ_n/Δ are expected to depend solely on the normalized coupling constant g/ω. We therefore plot Δ_n/Δ as functions of g/ω for all nine parameter sets together (Fig. 4). The parameters Δ, ω, and g are obtained from the transmission spectra. These results demonstrate huge Lamb shifts $|\Delta_0 - \Delta|$, some of them exceed 90% of the bare qubit frequencies Δ. These results also demonstrate that 1-photon and 2-photon ac-Stark shifts are so large that Δ_1 and Δ_2 change their signs depending on g/ω. The solid lines are theoretically predicted values given by Eq. (3). Table I shows a comparison between the measured and the numerically calculated Δ_n [29] using $\hat{H}_{\rm Rabi}$ and the parameters Δ, ω, and g. In many circuits, the measured Δ_2 is smaller than the numerically calculated one, while the agreement of Δ_0 and Δ_1 are good, with the deviations being at most 10 MHz. Since Δ_2 given by Eq. (3) is an approximation that becomes exact in the limit $\Delta/\omega \to 0$ while the numerically calculated Δ_2 is based on exact $\hat{H}_{\rm Rabi}$ for any set of parameters, the agreement of Δ_2 in Fig. 4 is a coincidence. In this way, our results can be used to check how well the flux qubit-LC oscillator circuits realize a system that is described by the quantum Rabi model Hamiltonian, which is the basis for several important applications, e.g. ultrafast gates [33] and quantum switches [34]. A possible source of the deviation in Δ_2 is higher energy levels of the flux qubit. As discussed in Ref. [17], the second or higher excited states can shift the energy levels of the qubit-oscillator circuit, even though there is an energy difference of at least 20 GHz between the first and the second excited states. Consideration of higher energy levels is necessary to identify the origin of the deviation in Δ_2.

In conclusion, we have used two-tone spectroscopy to study deep-strongly-coupled flux qubit-LC oscillator circuits. We have determined the energies of the six lowest energy eigenstates of each circuit and evaluated the photon-number-dependent qubit energy shifts. We have found Lamb shifts that exceed 90% of the bare qubit frequency, and inversions of the qubit's ground and excited states caused by the 1-photon and 2-photon ac-Stark shifts. The results agree with the quantum Rabi model, giving further support to the validity of the quantum Rabi model in describing these circuits in the deep-strong-coupling regime.

We thank Masahiro Takeoka for stimulating discussions. Z. A. acknowledges the Leading Graduate Program in Science and Engineering, Waseda University from MEXT, Japan. This work was supported by Japan Society for the Promotion of Science (JSPS) Grants-in-Aid for Scientific Research (KAKENHI) (No. JP25220601 and JP16K05497), and Japan Science and Technology Agency (JST) Core Research for Evolutionary Science and Technology (CREST) (Grant No. JPMJCR1775).

* fumiki@nict.go.jp
† semba@nict.go.jp

[1] W. E. Lamb and R. C. Retherford, Phys. Rev. **72**, 241 (1947).
[2] A. Blais, R.-S. Huang, A. Wallraff, S. M. Girvin, and R. J. Schoelkopf, Phys. Rev. A **69**, 062320 (2004).
[3] D. F. Walls and G. J. Milburn, Quantum optics (Springer Science & Business Media, 2007).
[4] R. J. Thompson, G. Rempe, and H. J. Kimble, Phys. Rev. Lett. **68**, 1132 (1992).
[5] A. Wallraff, D. I. Schuster, A. Blais, L. Frunzio, R.-S. Huang, J. Majer, S. Kumar, S. M. Girvin, and R. J. Schoelkopf, Nature **431**, 162 (2004).
[6] S. Kato and T. Aoki, Phys. Rev. Lett. **115**, 093603 (2015).
[7] M. Brune, F. Schmidt-Kaler, A. Maali, J. Dreyer, E. Hagley, J. M. Raimond, and S. Haroche, Phys. Rev. Lett. **76**, 1800 (1996).
[8] J. Johansson, S. Saito, T. Meno, H. Nakano, M. Ueda, K. Semba, and H. Takayanagi, Phys. Rev. Lett. **96**, 127006 (2006).
[9] D. J. Heinzen and M. S. Feld, Phys. Rev. Lett. **59**, 2623 (1987).
[10] M. Brune, P. Nussenzveig, F. Schmidt-Kaler, F. Bernardot, A. Maali, J. M. Raimond, and S. Haroche, Phys. Rev. Lett. **72**, 3339 (1994).
[11] A. Fragner, M. Göppl, J. M. Fink, M. Baur, R. Bianchetti, P. J. Leek, A. Blais, and A. Wallraff, Science **103**, 1357 (2008).
[12] D. I. Schuster, A. Wallraff, A. Blais, L. Frunzio, R.-S. Huang, J. Majer, S. M. Girvin, and R. J. Schoelkopf, Phys. Rev. Lett. **94**, 123602 (2005).
[13] D. Schuster, A. Houck, J. Schreier, A. Wallraff, J. Gambetta, A. Blais, L. Frunzio, J. Majer, B. Johnson, M. Devoret, et al., Nature **445**, 515 (2007).
[14] T. Niemczyk, F. Deppe, H. Huebl, E. P. Menzel, F. Hocke, M. J. Schwarz, J. J. Garcia-Ripoll, D. Zueco, T. Hümmer, E. Solano, A. Marx, and R. Gross, Nature Phys. **6**, 772 (2010).
[15] P. Forn-Diaz, J. Lisenfeld, D. Marcos, J. J. Garcia-Ripoll, E. Solano, C. J. P. M. Harmans, and J. E. Mooij, Phys. Rev. Lett. **105**, 237001 (2010).
[16] F. Yoshihara, T. Fuse, S. Ashhab, K. Kakuyanagi, S. Saito, and K. Semba, Nature Physics **13**, 44 (2017).
[17] F. Yoshihara, T. Fuse, S. Ashhab, K. Kakuyanagi, S. Saito, and K. Semba, Phys. Rev. A **95**, 053824 (2017).
[18] I. I. Rabi, Phys. Rev. **51**, 652 (1937).
[19] E. T. Jaynes and F. W. Cummings, Proceedings of the IEEE **51**, 89 (1963).
[20] D. Braak, Phys. Rev. Lett. **107**, 100401 (2011).
[21] S. Ashhab and F. Nori, Phys. Rev. A **81**, 042311 (2010).
[22] D. Z. Rossatto, C. J. Villas-Bôas, M. Sanz, and E. Solano, Phys. Rev. A **96**, 013849 (2017).
[23] J. E. Mooij, T. P. Orlando, L. Levitov, L. Tian, C. H. van der Wal, and S. Lloyd, Science **285**, 1036 (1999).
[24] J. Fink, M. Göppl, M. Baur, R. Bianchetti, P. Leek, A. Blais, and A. Wallraff, Nature **454**, 315 (2008).
[25] A. A. Abdumalikov, O. Astafiev, A. M. Zagoskin, Y. A. Pashkin, Y. Nakamura, and J. S. Tsai, Phys. Rev. Lett. **104**, 193601 (2010).
[26] H. Bloch and A. Siegert, Phys. Rev. **57**, 522 (1940).
[27] C. Cohen-Tannoudji, J. Dupont-Roc, and G. Grynberg, *Atom - Photon Interactions: Basic Process and Applications* (John Wiley and Sons, Inc., New York, 1992), Chap. 6.
[28] A. Zazunov, V. S. Shumeiko, G. Wendin, and E. N. Bratus', Phys. Rev. B **71**, 214505 (2005).
[29] See Supplemental Material [url] for (i) overlap between the displaced Fock states; (ii) symmetry of quantum Rabi model and state assignment from the spectra; (iii) coupler inductance and flux bias points; (iv) background transmission coefficient; (v) avoided crossings in two-tone spectroscopy; (vi) numerically calculated Δ_n, which includes Refs. [35, 36].
[30] J. Casanova, G. Romero, I. Lizuain, J. J. García-Ripoll, and E. Solano, Phys. Rev. Lett. **105**, 263603 (2010).
[31] X. Gu, A. F. Kockum, A. Miranowicz, Y. xi Liu, and F. Nori, Physics Reports **718-719**, 1 (2017).
[32] S. H. Autler and C. H. Townes, Phys. Rev. **100**, 703 (1955).
[33] G. Romero, D. Ballester, Y. M. Wang, V. Scarani, and E. Solano, Phys. Rev. Lett. **108**, 120501 (2012).
[34] A. Baust, E. Hoffmann, M. Haeberlein, M. J. Schwarz, P. Eder, J. Goetz, F. Wulschner, E. Xie, L. Zhong, F. Quijandría, D. Zueco, J.-J. G. Ripoll, L. García-Álvarez, G. Romero, E. Solano, K. G. Fedorov, E. P. Menzel, F. Deppe, A. Marx, and R. Gross, Phys. Rev. B **93**, 214501 (2016).
[35] M. S. Khalil, M. J. A. Stoutimore, F. C. Wellstood, and K. D. Osborn, Journal of Applied Physics **111**, 054510 (2012).
[36] J. R. Johansson, P. D. Nation, and F. Nori, Computer Physics Communications **184**, 1234 (2013).